Materials Horizons

ROYAL SOCIETY OF CHEMISTRY

COMMUNICATION

View Article Online
View Journal | View Issue

Check for updates

Cite this: *Mater. Horiz.*, 2025, **12**, 7012

Received 6th March 2025,
Accepted 6th June 2025

DOI: 10.1039/d5mh00408j

rsc.li/materials-horizons

Enhancing liquid–vapor phase behavior through multiscale anisotropic wettability gradient in dandelion-inspired nanostructures†

Jiayu Song,[a] Francis Eric P. Almaquer,[ab] Zixuan Xiong,[a] Xiong Wang,[c] Meng Li,[a] Xiao Yan,[d] Wei Han,[e] Qiong Wu,[a] Michael Kappl,[f] Youmin Hou,[g] Hans-Jürgen Butt[f] and King Lun Yeung*[ae]

Effective manipulation of liquid–vapor phase behavior is essential for advancing energy efficiency. This study presents a synthetic strategy for creating multiscale anisotropic wettability gradients through the assembly of dandelion-inspired nanostructures, achieving both horizontal (planar) and vertical biphilicity. This versatile approach is applicable to various nanowire materials, including silicon, zinc oxide, and copper oxide. Key findings demonstrate that these surfaces can be tuned to transit from jumping-droplet to dropwise and filmwise condensation while maintaining a stable Cassie state for the condensate. This configuration allows water droplets and films to float on the nanowire substrate, with dry nanowires beneath the water acting as vapor channels that promote droplet nucleation. Unlike traditional liquid film condensation, the ultrathin water film, measuring less than 2 μm in thickness, floats on the nanostructured surface, significantly reducing thermal resistance and enabling rapid condensate removal. The complex biphilic surfaces with a micro–nano–nano hierarchy effectively direct and organize water nucleation, facilitating controlled water flow and droplet departure from the surface. These findings underscore the potential of this innovative design to optimize liquid–vapor phase behaviors, offering transformative implications for enhanced heat transfer and fluid management in various applications.

New concepts

This study introduces a novel approach for enhancing liquid–vapor phase behavior through the development of multiscale anisotropic wettability gradients in dandelion-inspired nanostructures. Unlike traditional biphilic surfaces that primarily focus on planar wettability, our design achieves both horizontal and vertical biphilicity, allowing for a dynamic transition between jumping-droplet, dropwise, and filmwise condensation modes. This multifunctionality is made possible by the unique architecture of the nanostructures, which facilitates efficient water nucleation while maintaining a stable Cassie state, significantly reducing thermal resistance and promoting rapid condensate removal. The insights gained from this work extend the understanding of how hierarchical micro–nano structures can be engineered to optimize fluid management in thermal applications. Furthermore, our findings highlight the potential for tailoring surface properties through precise control of nanostructure morphology, paving the way for innovative applications in energy systems, microfluidics, and environmental technologies. This breakthrough not only enhances heat transfer efficiency but also provides a versatile framework for future research in materials science, focusing on the interplay between surface structure and liquid behavior.

1. Introduction

The liquid–vapor interface is a fundamental phenomenon present in nature and plays a crucial role in various energy

[a] *Department of Chemical and Biological Engineering, The Hong Kong University of Science and Technology, Clear Water Bay, Hong Kong, China. E-mail: kekyeung@ust.hk*
[b] *School of Technology, University of the Philippines Visayas, Miagao, Iloilo, 5023, Philippines*
[c] *Department of Mechanical Engineering, The Hong Kong Polytechnic University, Hong Kong, China*
[d] *Institute of Engineering Thermophysics, Key Laboratory of Low-grade Energy Utilization Technologies and Systems (Ministry of Education), Chongqing University, 400030, Chongqing, China*
[e] *Division of Environment and Sustainability, The Hong Kong University of Science and Technology, Clear Water Bay, Hong Kong, China*
[f] *Max Planck Institute for Polymer Research, Ackermannweg 10, 55128, Mainz, Germany*
[g] *School of Power and Mechanical Engineering, Wuhan University, 430072, Wuhan, China*

† Electronic supplementary information (ESI) available: Document S1: additional text and figures (Fig. S1–S14) describing materials characterizations and experimental details (DOCX); Video S1: dynamic water condensation behavior on the 2D biphilic dandelion-inspired nanostructures characterized by ESEM from the top-view; Video S2: dynamic water condensation behavior on the 2D biphilic dandelion-inspired nanostructures characterized by ESEM from the side-view; Video S3: cyclic water nucleation during the filmwise condensation on the 2D biphilic dandelion-inspired nanostructures characterized by ESEM from the side-view. See DOI: https://doi.org/10.1039/d5mh00408j

applications, particularly in thermal management.[1–3] One effective strategy for manipulating liquid–vapor phase behavior is by creating surfaces with heterogeneous wettability. This approach leverages the interplay between the surface energy of the substrate and the surface tension of the liquid, resulting in regions that exhibit either strong affinity for the liquid (hydrophilic) or repel it (hydrophobic). Such control allows for precise management of liquid transportation and phase-change processes. For instance, to enhance water condensation heat transfer efficiency, surfaces have been engineered to incorporate spatial hydrophilic domains within a superhydrophobic field, known as biphilic surfaces.[4] The hydrophilic regions facilitate water nucleation and growth, while the superhydrophobic background promotes droplet departure through coalescence-induced jumping. This innovative design has achieved over an 84% improvement in heat transfer coefficients compared to surfaces with uniform wettability.[5] Biphilic surfaces have demonstrated superior performance in various applications, including defrosting,[6] enhancing heat transfer efficiency during boiling,[7] and improving the hydrogen evolution rate.[8]

However, existing biphilic surfaces primarily concentrate on planar heterogeneous wettability or planar biphilicity. A notable limitation in water condensation applications arises from the hydrophilic regions, which facilitate nucleation but also lead to a Wenzel wetting state for droplets on these domains. This state results in increased adhesion forces that hinder droplet departure, thereby restricting the effective size and density of usable hydrophilic domains. A promising solution to this challenge is the introduction of vertical anisotropic wettability or vertical biphilicity. This design involves making the upper section of the structure hydrophilic while keeping the lower portion hydrophobic. Such a configuration promotes rapid vapor nucleation on the hydrophilic tops while maintaining a Cassie wetting state, which effectively reduces liquid adhesion.[4,9]

Vertical heterogeneous wettability (vertical biphilicity) also stands as a pivotal surface engineering strategy, especially for applications related to gas–liquid–solid involved reactions. For instance, in CO_2 reduction processes, pristine hydrophilic electrode surfaces experience complete wetting, leading to surface flooding that prevents CO_2 from reaching the electrode, which impedes reaction efficiency.[10] Conversely, superhydrophobic surfaces facilitate interfacial gas transport but limit the contact between the catalyst and the electrolyte for optimal catalytic performance. To address these challenges, studies have demonstrated that hydrophobic electrodes often outperform superhydrophobic and hydrophilic ones, primarily due to the partial wetting of the electrolyte on the electrode structures.[11,12] However, these works target the bulk electrocatalysts, impacting the hydrophobicity of the whole catalyst layer and lacking precise control of the wetting depth.[13,14] Thus, it is promising to explore the development of electrodes with vertical biphilicity, featuring two distinct regions within the catalyst layer: a hydrophobic bottom layer adjacent to the substrate and a hydrophilic upper layer near the liquid.

To achieve both horizontal and vertical biphilicity, this study introduces a dandelion-inspired nanostructure that enables the coexistence of superhydrophobicity and hydrophilicity along both the surface plane (horizontal biphilicity) and perpendicular to it (vertical biphilicity). The liquid–vapor phase behavior of these surfaces was investigated through water condensation experiments. When the surface area occupied by the dandelion-inspired nanostructures is minimal, the surface retains its superhydrophobicity, exhibiting jumping-droplet condensation. The vertical biphilicity of the structure allows droplets to experience reduced adhesion forces, leading to coalescence-induced jumping even at water contact angles below the critical threshold of 150°. As the coverage of these nanostructures increases, the surface transitions from hydrophobic to hydrophilic, showcasing both dropwise and filmwise condensation. The condensed water droplets and films adopt a Cassie state. In this Cassie state, the underlying dry nanowires function as vapor channels, providing sites for sustained water nucleation.

These condensates can be efficiently removed by the upper water film at significantly smaller scales (<5 μm) compared to the droplet departure sizes observed during either jumping-droplet or dropwise condensation processes. Furthermore, the thickness of the water film (<2 μm) is considerably less than that of the droplets formed during these condensation processes, resulting in lower heat transfer resistance. The water condensate can also be manipulated to create various patterns by selectively growing the dandelion-inspired nanostructures on the surface. This capability is enabled by a versatile fabrication strategy that allows the creation of these nanostructures using materials such as silicon, copper oxide, and titania.

2. Results and discussion

2.1. Two-dimensional biphilicity of dandelion-inspired surfaces

The dandelion-inspired two-dimensional (2D) biphilic surface was obtained by growing a hydrophilic cluster of ZnO nanorods on the tips of superhydrophobic silicon (Si) nanowires, following the steps outlined in Fig. 1(A). The Si nanowires were first fabricated using the Bosch deep reactive ion etching (DRIE) method, which involved cyclic etching and passivation steps. The resulting nanowires had a diameter of 240 ± 120 nm, a height of 6.7 ± 0.4 μm, and a pitch of 910 ± 170 nm (Fig. S1, ESI†). These nanowires were modified to achieve superhydrophobicity using 1*H*,1*H*,2*H*,2*H*-perfluorodecyltriethoxysilane, resulting in water contact angles of 164 ± 2° and sliding angles $<1°$ with the droplet volume of 7 ± 0.2 μL. The superhydrophobic Si nanowires were seeded with zinc acetate dispersed in ethanol. The seed suspension was spin-coated onto the substrate and then heated to 200 °C for 5 minutes. This process was repeated multiple times to increase the quantity of deposited seed particles. The seeded Si nanowire surface retained its superhydrophobicity and was subsequently treated with an aqueous precursor solution containing zinc nitrate and hexamethylenetetramine to grow ZnO nanorod clusters, as shown in

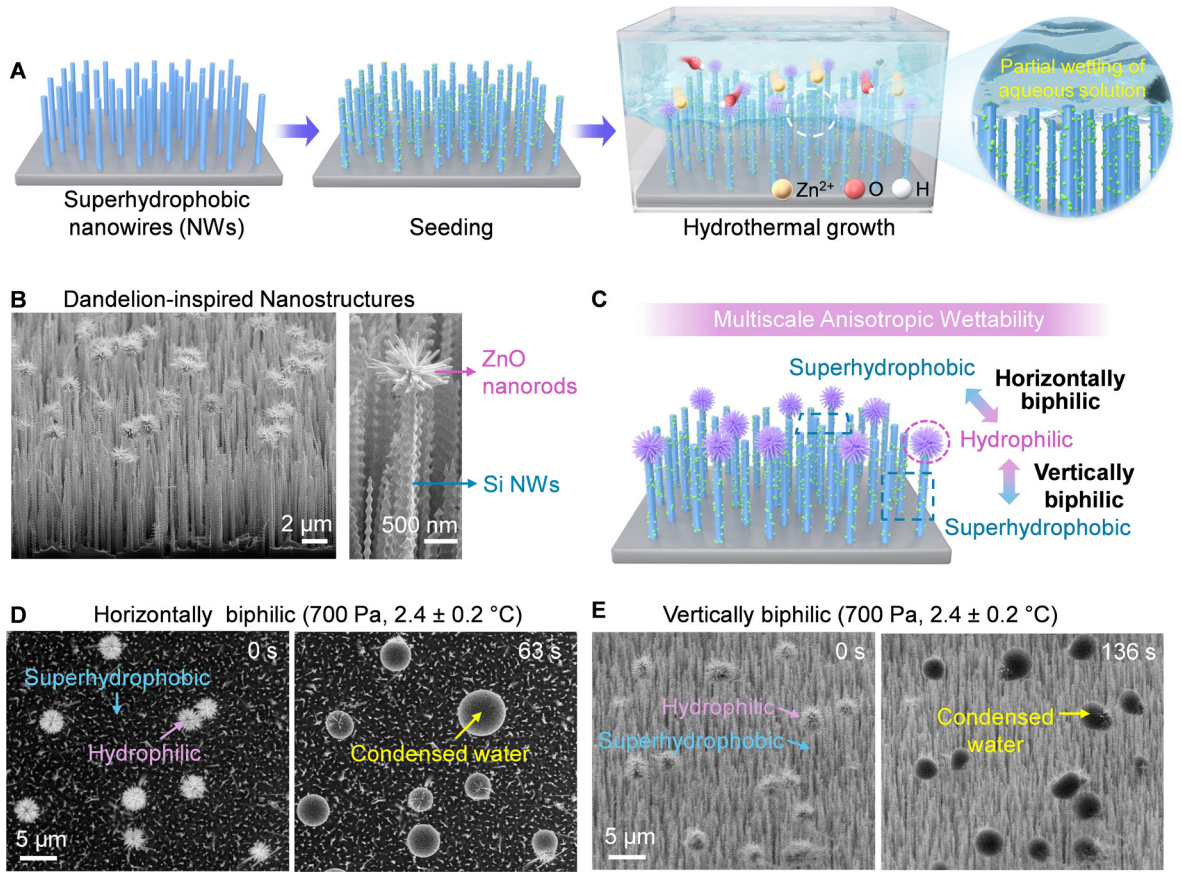

Fig. 1 Synthesis and biphilicity of the dandelion-inspired nanostructures. (A) Schematic representation of the synthesis procedure for growing dandelion-inspired nanostructures and (B) its corresponding images from environmental scanning electron microscopy (ESEM). (C) Schematic illustration of horizontal (planar) and vertical biphilicity of the nanostructures. (D) and (E) ESEM images providing visual confirmation of the biphilic characteristics of the surface: (D) horizontal biphilicity as observed from a top-down view, and (E) vertical biphilicity as observed from a side view, both during water condensation at a pure water vapor pressure of 700 Pa and a cooling stage temperature of 2.4 ± 0.2 °C.

Fig. 1(B). The scanning electron microscope (SEM) image shows that due to the limited wetting of the precursor solution, the hydrophilic ZnO nanorods grew exclusively on the tips of the seeded superhydrophobic Si nanowires. X-ray diffraction (XRD) and micro-Raman analyses confirmed that the nanowires were silicon and the dandelion-like clusters were wurtzite ZnO crystals, respectively (Fig. S2 and S3, ESI†). Detailed fabrication procedures are provided in the Materials and methods.

The water condensation on the biphilic nanostructures is illustrated in Fig. 1(C), which was conducted in an environmental scanning electron microscope (ESEM). The pure water vapor pressure in the ESEM chamber was maintained at 700 Pa. The cooling stage temperature was reduced to 2.4 ± 0.2 °C to initiate vapor condensation and droplet nucleation (for experimental details, see Materials and methods and Fig. S4, ESI†). These processes are recorded in Video S1 (ESI†) (top planar view) and Video S2 (ESI†) (cross-section tilted view). Fig. 1(D) and (E) present time-lapse ESEM images showing that water preferentially nucleates on the ZnO nanorod clusters on the tip of the superhydrophobic nanowires. As the water collects, it completely engulfs the clusters, forming spherical water droplets suspended away from the superhydrophobic surface (as highlighted by the yellow arrows in Fig. 1(D) and (E)). It demonstrates a multiscale anisotropic wetting with both planar (Fig. 1(D)) and vertical biphilicity (Fig. 1(E)).

The synthesis strategy presented here is versatile and can be applied to a variety of materials beyond silicon (Si) nanowires, including copper oxide (CuO) and titanium dioxide (TiO_2) nanowires, as illustrated in Fig. 2(A)–(C). These nanowires were synthesized as described in Materials and methods, and subsequently rendered superhydrophobic through treatment with 1*H*,1*H*,2*H*,2*H*-perfluorodecyltriethoxysilane. This was followed by the seeding and growth of ZnO nanorod clusters, as confirmed by scanning electron microscopy (SEM, Fig. 2(A)–(C)-(i)). The SEM results demonstrate the successful formation of dandelion-like microstructures on tips of Si, CuO, and TiO_2 nanowires. Elemental analysis *via* energy dispersive X-ray spectroscopy (EDXS) confirmed that the branches are composed of ZnO, while the nanowires are respectively Si, CuO, and TiO_2, as evidenced by the elemental maps (Fig. 2(A)–(C)-(ii)) and (Fig. S5, ESI†) and spectra (Fig. S6, ESI†).

The geometric configuration of the nanowires, such as spacing, alignment, and pitch, can significantly influence the formation and morphology of the ZnO nanorod clusters (Fig. 2).

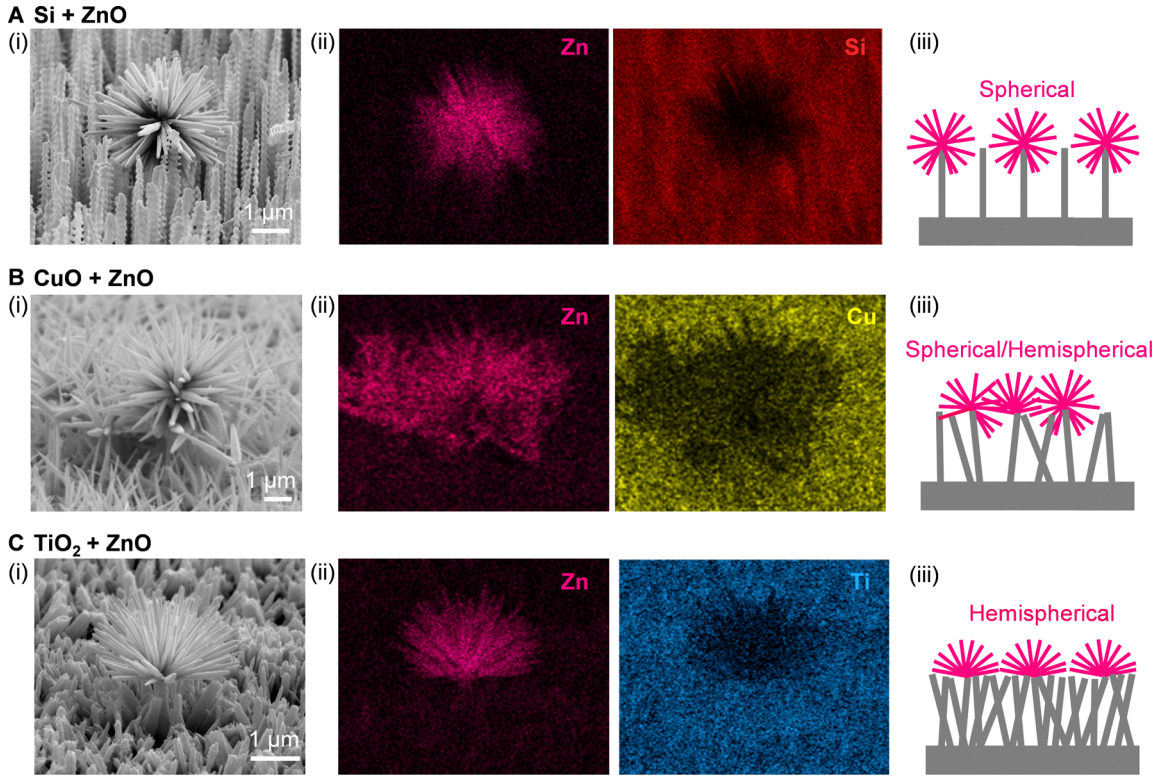

Fig. 2 Synthesis of the biphilic dandelion-inspired nanostructures on (A) Si, (B) CuO, and (C) TiO_2 nanowires. (i) SEM images, (ii) energy-dispersive X-ray spectroscopy (EDXS) elemental mapping of zinc (magenta), silicon (red), copper (yellow), and titanium (blue) elements, and (iii) schematic representations of the ZnO nanorod clusters on the various nanowires.

For the vertically aligned Si nanowires, when the length of the ZnO nanorods (1.4 ± 0.10 μm) is comparable to the distances between nanowires (0.91 ± 0.17 μm), a spherical ZnO nanorod cluster is formed (Fig. 2(A)). In contrast, the randomly tilted CuO nanowires exhibit greater variability in inter-nanowire distances, averaging 0.99 ± 0.44 μm, with some gaps reaching as large as 2.1 μm. These larger gaps facilitate the infiltration of synthesis solutions, resulting in the formation of spherical ZnO nanorod clusters. Conversely, the smaller gaps hinder the precursor penetration, leading to hemispherical ZnO nanorod clusters, as shown in Fig. 2(B).

For TiO_2 nanowires, a hemispherical morphology of the ZnO nanorod clusters is observed because the nanorod length (1.7 μm $\pm$ 0.28 μm) significantly exceeds the gap distance (0.34 ± 0.13 μm) (Fig. 2(C)). Importantly, the resulting biphilic nanostructures derived from CuO and TiO_2 nanowires also exhibited the desired horizontal (planar) and vertical biphilic properties, demonstrating selective water nucleation and droplet formation on the hydrophilic ZnO nanorod clusters (Fig. S7, ESI†).

The horizontal biphilicity changes with the number and size of the hydrophilic ZnO nanorod clusters by adjusting the seeding parameters (Fig. 3(A)), including seed concentration and the number of seeding cycles, as well as the hydrothermal synthesis time (Fig. 3(B)). Higher concentrations of seed solutions and an increased number of seeding cycles resulted in a greater density of ZnO nanorod clusters per unit area (ρ), as demonstrated in Fig. 3(C).[15,16] For the surface to exhibit biphilic properties, it is essential to maintain anisotropic wetting characteristics, with hydrophilic nanorod clusters localized exclusively at the tips of the superhydrophobic Si nanowires, as depicted in the inset of Fig. 3(A)-(viii). However, excessive seeding can lead to complete coverage of the superhydrophobic nanowires with hydrophilic ZnO seeds. This coverage can render the surface predominantly hydrophilic, allowing the synthesis solution to penetrate deeply into the nanowire layer. As a result, ZnO nanorods may grow along the entire length of the nanowires, as illustrated in the inset of Fig. 3(C)-(ix). This growth transforms the entire outer surface of the nanowires into a hydrophilic state, resulting in isotropic wetting properties. This observation highlights the delicate balance required in the seeding process to achieve the desired anisotropic wettability while preserving the superhydrophobic characteristics of the surface.

It is important to note that, for surfaces subjected to the same hydrothermal growth time (as shown in Fig. 3(A)), an increase in cluster density (ρ) is associated with a decrease in branch length (L), as indicated by the blue dots in Fig. 3(D). This inverse relationship can be understood through the principles of competitive growth: as more nucleation sites are created with more seeds, the available resources for individual nanorod growth become limited, resulting in shorter branch lengths. Conversely, extending the synthesis time allows for the growth of longer ZnO nanorods, as observed in Fig. 3(B) and

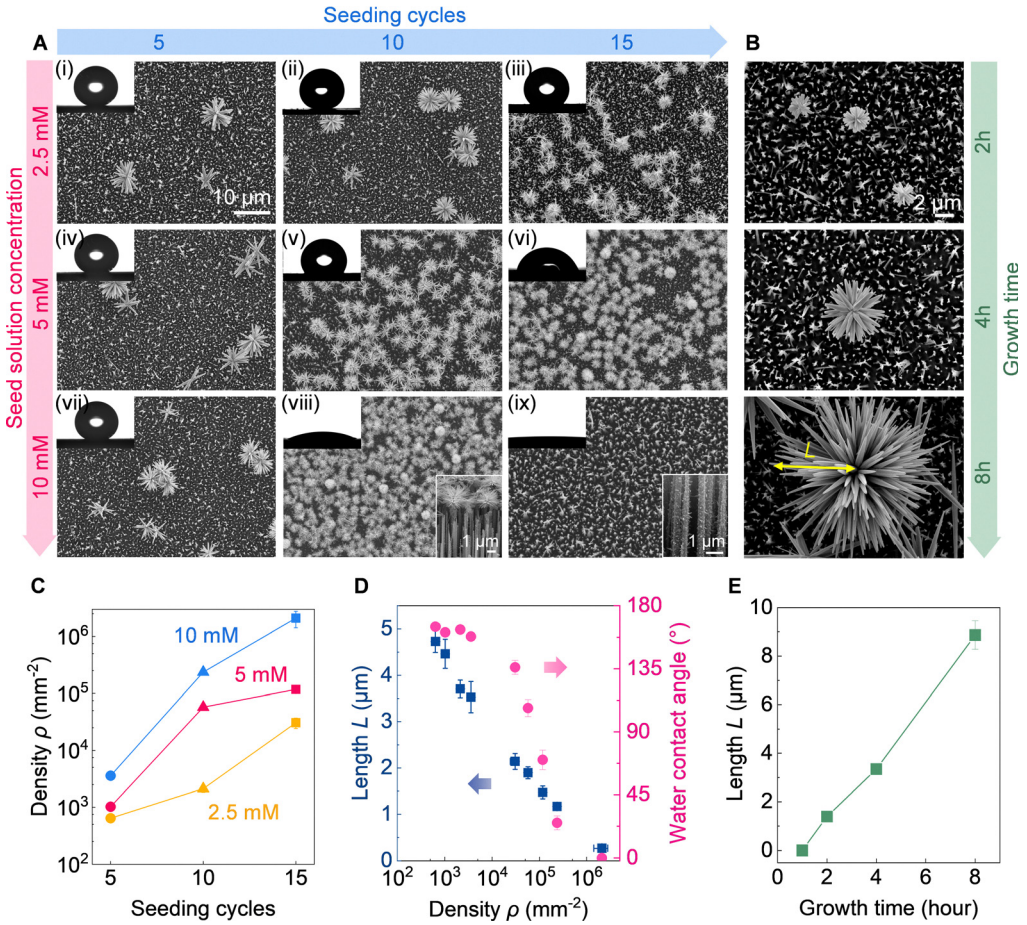

Fig. 3 Influence of synthesis parameters on surface morphology and wettability of the biphilic dandelion-inspired nanostructures. SEM images and water contact angle measurements (inset) of (A) surfaces prepared with varying seeding conditions while maintaining a 4 h hydrothermal synthesis time and (B) surfaces with different hydrothermal growth time, with the surface seeded five times from 10 mM seed solutions. Plots of (C) the dandelion-like cluster density (ρ) from 2.5 mM (yellow), 5 mM (magenta), and 10 mM (blue) seed solutions for 5 (○), 10 (△), and 15 (□) times of seeding; (D) the correlation between ZnO nanorod length (L), water contact angle, and ρ; (E) the variation of nanorod length L with hydrothermal growth time.

plotted in Fig. 3(E), by providing more time for the nanorods to grow. Thus, the surface coverage (α) of hydrophilic ZnO nanorod clusters is calculated from eqn (1), assuming the clusters are non-overlapping and circular with a radius equal to the length of the ZnO nanorods (L), as indicated by the yellow arrow in Fig. 3(B).

$$\alpha = \pi L^2 \rho \quad (1)$$

These values are plotted against ρ in Fig. S8 (ESI†).

The wettability of these surfaces was characterized using the sessile droplet method, with a water droplet volume of 7 ± 0.2 μL, as shown in the insets of Fig. 3(A). At low ρ, indicating a small coverage ratio of the hydrophilic ZnO nanorod clusters, the surfaces remained predominantly superhydrophobic. As ρ increased, the surface gradually transitioned toward hydrophilicity, as illustrated by the pink dots in Fig. 3(D). The surface with nearly complete cluster coverage (α = 0.96, Fig. 3(A)-(viii)) achieved the lowest water contact angle of 25 ± 5°. Superhydrophilicity, characterized by a contact angle of 0°, was observed when ZnO branches grew across the entire surface of the nanowires (Fig. 3(A)-(ix)). The transition from superhydrophobic to superhydrophilic highlights the potential of this technique for tailoring surface wettability.

2.2. Water condensation on the 2D biphilic surfaces

The 2D biphilic surfaces with varying densities (ρ) and lengths (L) of ZnO nanorod clusters were synthesized to investigate their water condensation behavior using environmental scanning electron microscopy (ESEM).[17–21] Fig. 4(A)–(C) illustrate three distinct condensation processes observed on these surfaces: jumping-droplet condensation, dropwise condensation, and filmwise condensation.

The surfaces characterized by a low coverage of the hydrophilic clusters (α < 0.15), as shown in Fig. S9A (ESI†), were superhydrophobic with water contact angles of 161 ± 2° and contact angle hysteresis of 2 ± 1°. On these surfaces, condensed droplets demonstrated spontaneous jumping following droplet coalescence (Fig. 4(A)). Jumping-droplet condensation occurs due to the excess surface free energy associated with droplet coalescence on the hydrophobic surface.[22] The surface exhibits

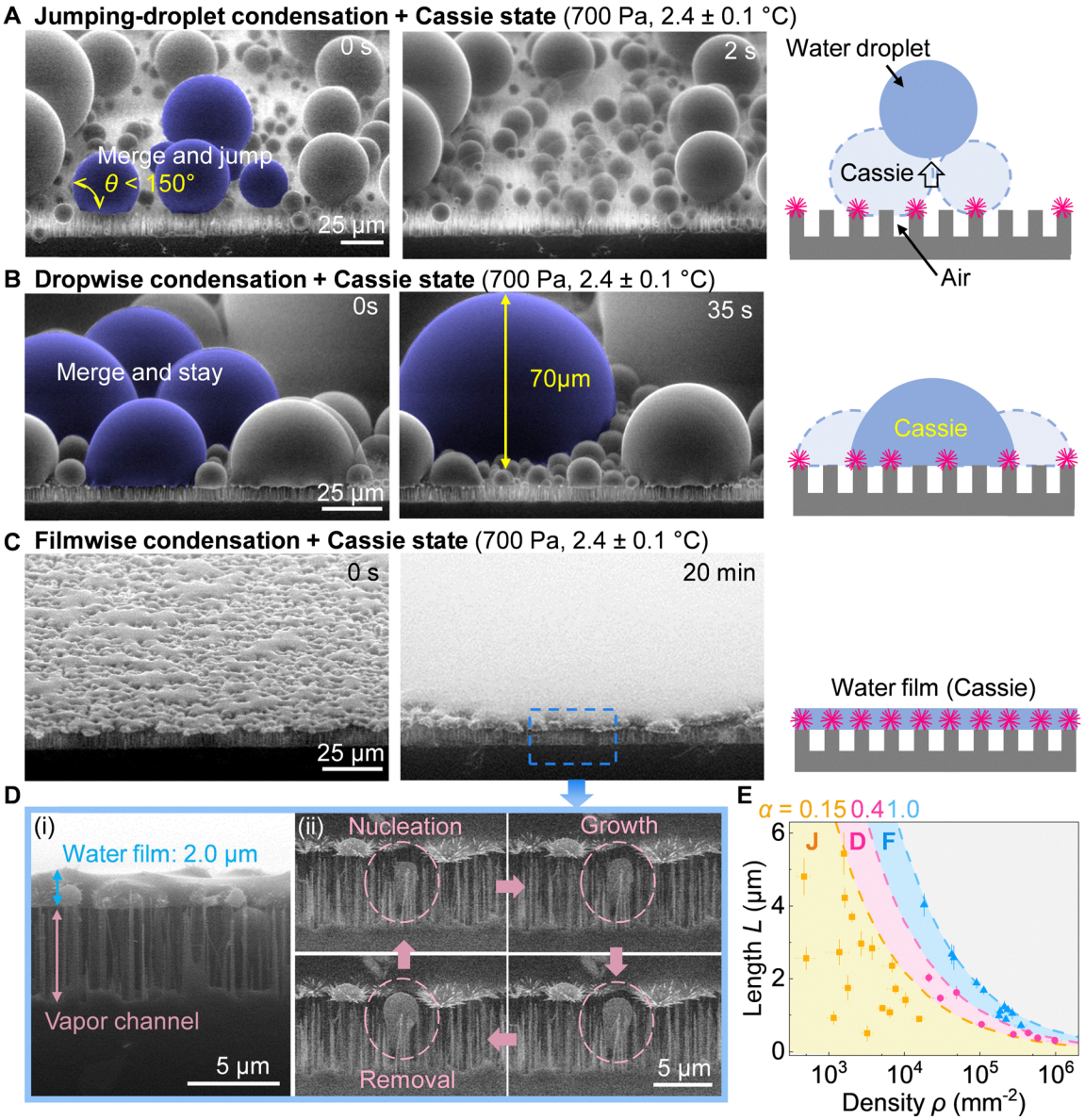

Fig. 4 Water condensation on 2D biphilic surfaces. Time-lapse ESEM images and schematic illustrations of water condensation on surfaces with (A) α = 0.09 and jumping droplet condensation, where condensed droplets merge and subsequently jump off the surface. Water droplets with θ less than the threshold 150°, highlighted in yellow in the ESEM image at 0 s, also exhibit jumping behavior after merging; (B) α = 0.36 and dropwise condensation under Cassie wetting state; (C) α = 0.97 and filmwise condensation under Cassie wetting state, revealing (D) (i) the Cassie state of the thin condensed water film (thickness <2 μm) and (ii) cyclic water nucleation occurring beneath the liquid film. (E) A summary of water condensation behaviors with α values of <0.15 (yellow), 0.4 (magenta), and 1.0 (blue). ESEM observations were conducted under pure water vapor conditions at a vapor pressure of 700 Pa and a cooling stage temperature of 2.4 ± 0.1 °C.

a higher water nucleation density and jumping frequency than uniform superhydrophobic surfaces, as shown in Fig. S10 (ESI†). This enhancement can be attributed to the hydrophilic regions, which lower the energy barrier for water nucleation, while the surrounding superhydrophobic areas maintain sufficient water repellency to facilitate droplet jumping.[23] Notably, droplets with contact angles (θ) lower than 150° also exhibited self-departure through coalescence-induced jumping, highlighted in yellow in Fig. 4(A). This observation is significant as the minimum contact angle for droplet jumping is typically around 150°.[24] This unique feature is due to the vertical biphilic characteristics, allowing the condensate on the hydrophilic clusters to adopt a Cassie-like state. This substantially reduces the work of adhesion compared to condensate in the partial-Wenzel state on the superhydrophobic area[9] (Fig. S11, ESI†) or condensate in the Wenzel state on the hydrophilic or hydrophobic sites of conventional biphilic surfaces.[4] Therefore, water droplets on the 2D biphilic surfaces require less excess surface free energy to initiate self-propelled jumping, resulting in smaller critical water contact angles for droplet departure.

When the surface coverage reached 0.15 < α < 0.4 (Fig. S9B, ESI† with water contact angles of 106 ± 4° and contact angle

hysteresis of 73 ± 6°), the condensed water droplets experienced stronger pinning forces, leading to their retention on the surface after merging. This behavior is characteristic of dropwise condensation, as illustrated in Fig. 4(B). ESEM images from the side view revealed that these droplets, despite having water contact angles below 90°, rested upon the nanowires with air pockets confined between them, exhibiting the Cassie mode of wetting. In the Cassie state, the liquid droplets sit on top of the surface texture, which includes both solid and air, effectively reducing the contact area between the liquid and the solid substrate. This unique wetting configuration minimizes adhesive forces between the droplet and the surface, facilitating droplet mobility and enhancing overall condensation efficiency. Maintaining the Cassie state under these conditions is vital for enhancing heat transfer, as it not only promotes rapid droplet departure but also aids in the nucleation of new droplets. The air pockets beneath the droplets decrease the effective contact area, lowering the energy barrier for detachment and allowing the droplets to more easily overcome pinning forces. Increasing the cluster coverage to $\alpha = 0.97$ (Fig. S9C, ESI†) led to the formation of a continuous water film, indicating filmwise condensation (Fig. 4(C)). In contrast to conventional filmwise condensation, where the water film completely wets the nanostructures in a Wenzel state (Fig. S12, ESI†), the water film on the 2D biphilic surface floated on the nanowires, exhibiting the Cassie state (Fig. 4(D)-(i)).

To assess the potential for enhancing condensation heat transfer, the water condensation efficiency of the three 2D biphilic surfaces (Fig. 4(A)–(C)) exhibiting jumping-droplet condensation, dropwise condensation, and Cassie state filmwise condensation (referred to as Filmwise (Cassie)) was characterized by a custom-built setup (see Fig. S13 for experimental details, ESI†). The filmwise condensation with Wenzel state (Filmwise (Wenzel)) was also evaluated on the superhydrophilic silicon nanowire surface (Fig. S12, ESI†). As shown in Fig. S14 (ESI†), jumping-droplet condensation showed the highest efficiency due to the rapid droplet removal, followed by dropwise condensation and Filmwise (Wenzel), consistent with previous studies.[5,19] However, by introducing vertical biphilicity, we observed that Filmwise (Cassie) achieved a condensation flux comparable to dropwise condensation and 16% higher than Filmwise (Wenzel). We attribute this phenomenon to the architecture of a thin (~2 μm) liquid film floating on superhydrophobic nanowires. The bottom dry nanowire substrate serves as a gas channel for water vapor diffusion and nucleation (Fig. 4(D)-(ii) and Video S3, ESI†), which is advantageous for improving condensation heat transfer efficiency according to our theoretical analysis presented in Fig. S15 (ESI†). The top water film allows for the effective collection and drainage of water condensates at much smaller scales (diameters <5 μm) compared to the average droplet departure size (diameters >20 μm) during jumping-droplet condensation.[4,23,25,26] Furthermore, the thickness of the water film on the 2D biphilic surface can be reduced to less than 2 μm (Fig. 4(D)-(i)), significantly thinner than the droplet diameters observed in dropwise and jumping-droplet condensations (tens of micrometers[27–29]), resulting in less thermal resistance. The thickness of the water film can be adjusted by varying the hydrophilic branch length, with longer branches producing a thicker liquid film (Fig. S16, ESI†). The height of the gas channel is also tunable by changing the height of the superhydrophobic nanowires. Future exploration could be done to investigate the structural parameter effects on condensation heat transfer efficiency of the 2D biphilic surfaces and to evaluate the stability of the Cassie state under extreme condensation conditions.

The dandelion-like morphology demonstrates resilience during water condensation, showing no significant reduction in the area covered by ZnO after 7 days of continuous operation. However, a slight decrease in ZnO branches was observed in incompletely formed dandelion clusters under jumping-droplet condensation (Fig. S17, ESI†). Furthermore, hydrophilic nanomaterials can become hydrophobic due to the adsorption of ambient volatile organic compounds (VOCs).[30] Under UV irradiation, ZnO effectively photodegrades these compounds, allowing for the regeneration of hydrophilic branches after contamination.[30] Additionally, the inherent antimicrobial properties of ZnO contribute to its functional longevity.[30] Together, these features ensure the long-term stability of the 2D biphilic surfaces during water condensation.

Fig. 3(E) provides a comprehensive overview of the condensation modes on the surfaces with varying surface coverage (α) of dandelion nanorod clusters. More clusters and longer nanorods see the transition from jumping-droplet condensation to dropwise condensation and, ultimately, to filmwise condensation. When α is less than 0.15 (the region to the left of the yellow dashed line in Fig. 4(E)), the surfaces exhibit jumping-droplet condensation. In the range of $0.15 < \alpha < 0.4$ (between the magenta and yellow dashed lines), dropwise condensation is observed. Further increases in α lead to filmwise condensation, with the blue dashed line ($\alpha = 1.0$) indicating that the surface is completely covered by the hydrophilic dandelion clusters and exhibits superhydrophilicity.

2.3. Complex micropatterning of dandelion-inspired nanostructures

Regarding horizontal biphilicity, the hydrophilic domains displayed a random distribution on flat nanowire substrates (Fig. 1). To overcome this limitation, we developed strategies to achieve spatial control over the location of hydrophilic sites, as illustrated in Fig. 5(A). The process begins with the fabrication of microstructures on a substrate, followed by the growth of nanowires on the micropatterned surface. This is demonstrated for a laser-etched copper surface shown in Fig. 5(B), which features regularly spaced conical structures with a pitch of 15 ± 1 μm and a height of 6 ± 1 μm, arranged in a square grid pattern (Fig. S18, ESI†). The entire surface is then covered with superhydrophobic CuO nanowires (see Materials and methods). Selective seeding and growth guide the formation of hydrophilic dandelion-like ZnO nanorod clusters, specifically at the apex of the conical structures, as illustrated in Fig. 5(C), which includes an overlay of the EDXS Zn elemental map. Notably, the growth of these hydrophilic clusters is

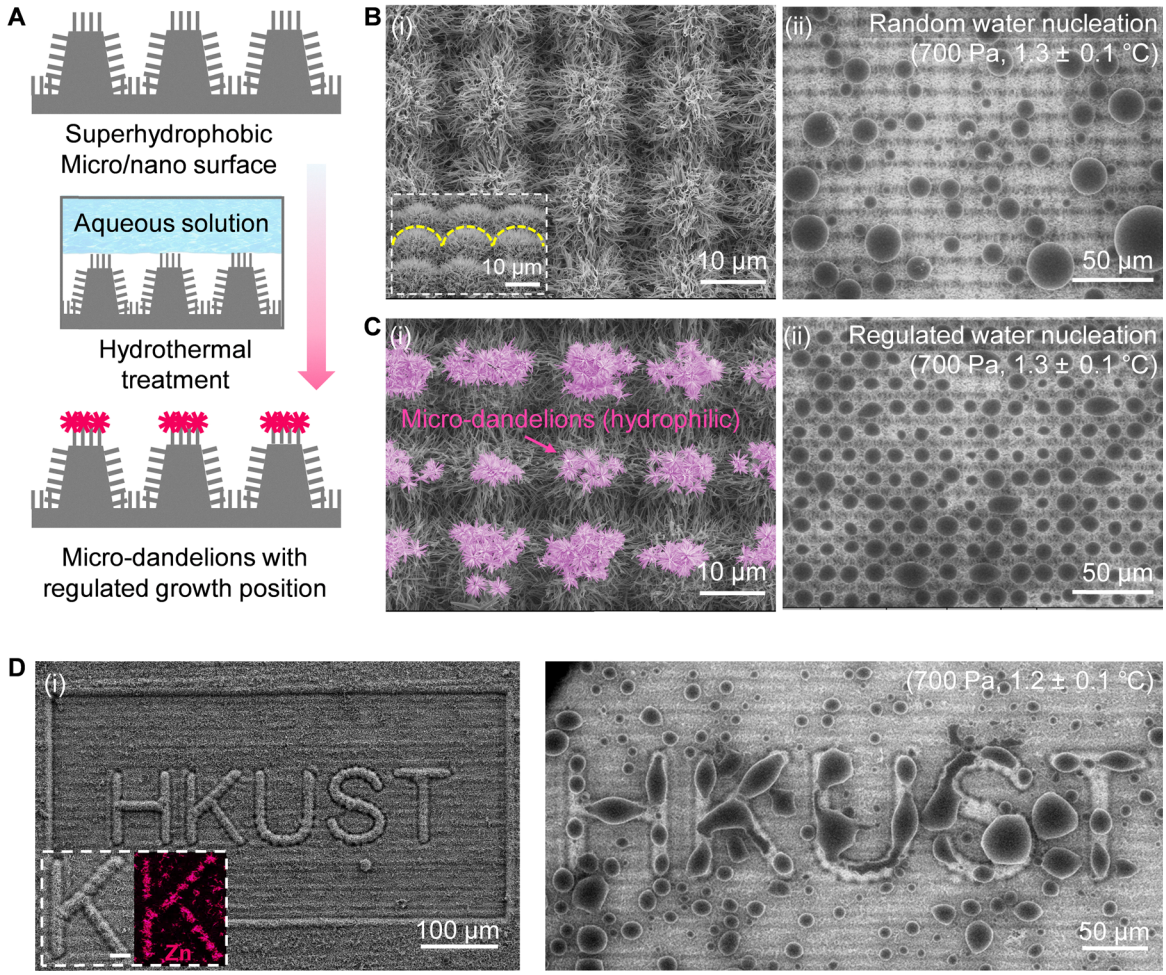

Fig. 5 Micropatterning of the biphilic nanostructures. (A) Schematic illustration of the fabrication procedure. (B) (i) SEM images of a micropatterned copper surface featuring a micro–nano hierarchical structure with CuO nanowires on conical microstructures (yellow dashed line in inset), and (ii) the corresponding water condensation behavior observed under ESEM. (C) (i) SEM images of the patterned surface showing selective growth of hydrophilic dandelion clusters, forming a micro–nano–nano hierarchy at the apex of the conical structures, and (ii) ESEM observation of water condensation on it. (D) (i) SEM image of a patterned multiscale anisotropic wettability gradient surface shaped like the HKUST logo, including insets of a magnified SEM image and the corresponding EDXS map of the Zn element, and (ii) ESEM image illustrating water condensation behavior. Note: ESEM water condensation experiments were conducted at an environmental pure water vapor pressure of 700 Pa and a cooling stage temperature of 1.2 ± 0.1 °C.

confined to the tips of the cones because the superhydrophobic CuO nanowires create a barrier that suspends the growth solution above the surface, preventing it from penetrating and allowing growth on the rest of the cones.

Water condensation study in ESEM demonstrates that water nucleation is highly localized and organized on the micropatterned multiscale anisotropic wettability gradient surfaces. As shown in Fig. 5(C)-(ii), nucleation primarily occurs on the hydrophilic dandelion clusters at the apex of the conical structures, resulting in a distinct and orderly pattern of water condensate. In contrast, on uniform superhydrophobic micro/nano surfaces, water nucleation appears random, as depicted in Fig. 5(B)-(ii). This localized nucleation behavior on the micropatterned surfaces can be attributed to the unique combination of hydrophilic and hydrophobic regions, which promotes efficient condensation by facilitating droplet formation at specific sites. The ability to control the nucleation patterns on surfaces represents a promising approach for effective fluid management and energy efficiency.

To explore the potential for creating intricate condensate patterns, the concept was extended to fabricate a 2D biphilic surface in the shape of linear arrays (Fig. S19, ESI†) and the HKUST logo (Fig. 5(D)-(i)). For the HKUST pattern, the fabrication began with laser ablation, which patterned the logo onto a copper plate by carving out the surrounding material to a depth of 10 μm (see Fig. S20, ESI†). Subsequently, CuO nanowires were grown on this microstructure, and the surface was treated to achieve a superhydrophobic state. The treated surface was then seeded and exposed to a zinc aqueous precursor solution for the hydrothermal growth of ZnO nanorod clusters. The EDXS Zn elemental map (inset in Fig. 5(D)-(i)) confirmed that the dandelion clusters predominantly formed on the letters of the logo, with sparse clusters also observed in the lower sections of the pattern. Water condensation behavior on this

surface demonstrated a clear preference for nucleation on the tops of the 'HKUST' logo, as shown in Fig. 5(D)-(ii). These findings underscore the ability to achieve complex biphilic surfaces through the controlled assembly of nanostructures.

3. Conclusions

This study successfully demonstrates the fabrication and functionality of multiscale anisotropic wettability gradient surfaces inspired by dandelion-like nanostructures. By achieving both horizontal and vertical biphilicity, we have shown that these surfaces can effectively manipulate liquid–vapor phase behavior, transitioning seamlessly between jumping-droplet, dropwise, and filmwise condensation modes. The maintenance of a stable Cassie state allows for the efficient management of condensate behavior, with water droplets and films floating on the nanowire substrate, facilitated by underlying dry nanowires that act as vapor channels.

The densities and nanorod lengths of hydrophilic dandelion-like ZnO nanorod clusters can be finely tuned by varying the seeding conditions and hydrothermal treatment time to obtain different surface coverages, a. When a is low (<0.15), the surface exhibits efficient jumping-droplet condensation, with condensates demonstrating coalescence-induced jumping even at water contact angles below 150°. As a increases ($0.15 < \alpha < 0.4$), the condensation behavior transitions from jumping-droplet to dropwise and ultimately to filmwise condensation as a approaches 1.0. The ultrathin water film, measuring less than 2 μm in thickness, significantly reduces thermal resistance, enabling rapid condensate removal and enhancing overall heat transfer efficiency. The ability of these complex surfaces to direct and organize water nucleation represents a significant advancement in the field, providing a powerful tool for optimizing fluid management and thermal processes.

Moreover, the versatility of this synthetic strategy, which is applicable to various nanowire materials such as silicon, zinc oxide, and copper oxide, opens new avenues for research and development in microfluidics,[31–33] thermal management,[34,35] and energy systems.[36,37] Additionally, other forms and materials can be utilized to construct diverse biphilic structures, further enhancing system performance. Future work will focus on exploring additional applications of these biphilic surfaces, including their potential in energy harvesting,[38] catalysis,[39–41] and environmental technologies.[42,43] Overall, the findings of this study provide valuable insights into the design of advanced surfaces that enhance liquid–vapor interactions, paving the way for innovative solutions across a range of scientific and engineering disciplines.

4. Materials and methods

4.1. Synthesis of Si nanowires

Si nanowires were fabricated on p-type Si(100) wafers (Micro-Chemicals GmbH, Germany) using a modified Bosch deep reactive ion etching (DRIE) method.[23] This process involved alternating cycles of anisotropic etching with SF_6 (99.99%, Linde) and O_2 (99.999%, Linde), and passivation using C_4F_8 (99.995%, Linde). The fabrication was conducted in an inductively coupled plasma DRIE system (Surface Technology Systems, UK) under 27 ± 2 mTorr vacuum and 20 °C. A single processing cycle started with an 8.5-second passivation step, during which the plasma was generated with a coil power of 700 W, a platen power of 0 W, and a C_4F_8 gas flow rate of 180 sccm. This was followed by a 7-second etching, wherein the coil power remained at 700 W, while the platen power was set to 16 W, with SF_6 and oxygen (O_2) gas flow rates of 130 sccm and 13 sccm, respectively. After 80 consecutive processing cycles, uniform Si nanowires were successfully obtained on the 525 μm Si wafers, which were used as received without additional pretreatment prior to the DRIE process.

4.2. Synthesis of TiO_2 nanowires

Titanium plates (>99%, Baotai Co. Ltd, China) were cut into 3×4 cm^2 pieces and cleaned through a 10-min ultrasonication in acetone (>99.8%, Sigma-Aldrich). Residual liquid was removed by blowing dry N_2. The plates were then placed on a ceramic holder and calcined at 700 °C for 6 h, with a heating rate of 3 °C min^{-1} using a muffle furnace (Carbolite CWF 11/13, UK). TiO_2 nanowires were synthesized *via* a hydrothermal method. A 60 mL solution of 6 M hydrochloric acid was prepared by diluting concentrated HCl (37%, VWR) with deionized distilled water in a 1 : 1 volume ratio. This acid was mixed with 0.9 mL of titanium isopropoxide (97%, Sigma-Aldrich) and stirred for 30 minutes. The resulting mixture was then transferred to a 125 mL Teflon-lined stainless-steel autoclave, where the previously calcined titanium plate was immersed, ensuring the preferred side for nanowire growth faced down to prevent TiO_2 particle precipitation. The autoclave was heated to 150 °C for 24 h using an electric oven (Memmert UN55, Germany). After cooling, the sample was removed, washed with deionized water, and blow-dried. Finally, the titanium nanowire sample was annealed at 450 °C for 2 h with a heating rate of 3 °C min^{-1} using the muffle furnace, resulting in uniform TiO_2 nanowires on the titanium plates (see Fig. S1, ESI† and Fig. 4(C)).

4.3. Synthesis of CuO nanowires

Copper plates (>99.99%, Xinhe Co. Ltd, China) were cleaned by ultrasonication in acetone (>99.8%, Sigma-Aldrich) for 10 minutes, followed by rinsing in absolute ethanol (99.97%, VWR) and deionized distilled water. After blow-drying with N_2, two separate solutions were prepared: 30 mL of 0.2 M ammonium persulfate (≥98%, Sigma-Aldrich) and 30 mL of 5.0 M sodium hydroxide (≥98%, Sigma-Aldrich), both cooled to 10 °C. The solutions were mixed by stirring for 5 minutes while maintaining the temperature. The cleaned copper plates were immersed in this mixture for 10 minutes, then thoroughly washed with deionized water and heated at 180 °C for 3 h in an electric oven (Memmert UN55, Germany), resulting in uniform CuO nanowires on the copper substrates.

4.4. Synthesis of superhydrophobic nanowire surfaces

Superhydrophobic nanowire surfaces were obtained by treating hydrophilic nanowires with low surface energy materials, specifically 1*H*,1*H*,2*H*,2*H*-perfluorodecyltriethoxysilane (97%, Sigma-Aldrich). A solution was prepared by mixing 200 μL of this silane with 50 mL of hexane (anhydrous 95%, Sigma-Aldrich) while stirring at 200 rpm for 2 minutes. The nanowire samples were fully immersed in this solution for 1 h, then removed and washed three times with 200 mL of hexane. The samples were subsequently heated to 140 °C for 1 h, resulting in superhydrophobic surfaces with water contact angles exceeding 155°.

4.5. Synthesis of the biphilic dandelion-inspired nanostructures

To create the 2D biphilic surfaces, hydrophilic ZnO nanorods were grown in ZnO-seeded superhydrophobic nanowires using an aqueous precursor solution. Zinc acetate dihydrate (reagent grade, Sigma-Aldrich) was dissolved in absolute ethanol (99.97%, VWR) at concentrations ranging from 2.5 to 10 mM to deposit seeds on the superhydrophobic nanowires. A spin coater (IMECAS KW-4T, China) was employed to ensure uniform coverage of the seed solution, dispensing 0.3 mL onto the nanowire surface (1 × 2 cm^2) at a speed of 1000 rpm for 20 s. The sample was then heated in a 200 °C oven for 5 minutes to yield ZnO seeds. Seeding was repeated 5, 10, and 15 times for different samples to study its effect on the dandelion morphology. A precursor solution was prepared by mixing 30 mL of 20 mM zinc nitrate hexahydrate (98%, Sigma-Aldrich) with 30 mL of 20 mM hexamethylenetetramine (≥99.0%, Sigma-Aldrich) and stirring for 15 minutes in a 125 mL Teflon-lined stainless-steel autoclave. The seeded samples were immersed in the precursor solution with the preferred side for ZnO growth facing down, and the autoclave was heated at 95 °C for 1–8 h. After cooling to room temperature, the samples were washed four times with 100 mL of deionized distilled water and dried at 60 °C for 24 h, yielding dandelion-like nanorod clusters on the nanowire surfaces.

4.6. Fabrication of micro/nanostructures on Cu plates

Microstructures on the Cu substrate were created using a femtosecond laser (Amplitude, France) with a spot diameter of approximately 10 μm, a repetition rate of 200 kHz, and a power of 3 W. The scanning process was repeated 55 times at a velocity of 2000 mm s^{-1}. The resulting microstructured copper substrate was cleaned by ultrasonication in acetone (>99.8%, Sigma-Aldrich) for 10 minutes, followed by rinsing with absolute ethanol (99.97%, VWR) and blow-drying with N_2. Two separate solutions were prepared: 30 mL of 0.2 M ammonium persulfate (≥98%, Sigma-Aldrich) and 30 mL of 5.0 M sodium hydroxide (≥98%, Sigma-Aldrich), both cooled to 10 °C. These solutions were mixed by stirring for 5 minutes at the same temperature. The cleaned microstructured copper plate was immersed in this mixture for 10 minutes, thoroughly washed with deionized water, and heated at 180 °C for 3 h in an electric oven (Memmert UN55, Germany), resulting in a uniform micro/nanostructured copper plate. This fabricated plate was then treated with low surface energy materials, specifically 1*H*,1*H*,2*H*,2*H*-perfluorodecyltriethoxysilane (97%, Sigma-Aldrich), in a manner similar to the nanowire surfaces, achieving superhydrophobic characteristics after immersion in a solution of 200 μL of silane mixed with 50 mL of hexane for 1 h, followed by washing and heat treatment at 140 °C for 1 h.

4.7. Water condensation study using environmental scanning electron microscopy (ESEM)

The nucleation and growth of water on the synthesized surfaces were investigated using environmental scanning electron microscopy (ESEM, FEI Quanta 250 FEG, USA). Samples were mounted on a copper holder using silver conductive paint (SPI supplies, USA) and placed on a Peltier cooling stage. The electron beam voltage was set to 8 keV, with a working distance of 6 cm. The ESEM chamber was evacuated to remove non-condensable gases before introducing pure water vapor, maintaining a vapor pressure of 700 Pa during observations. The sample surface was gradually cooled at a rate of 5 °C min^{-1} to induce water condensation, with a tilting angle of 75° for side view observations.

4.8. Instrumentation

Surface morphology and chemical composition were analyzed using a scanning electron microscope (JEOL JSM-7100F, Japan) equipped with energy-dispersive X-ray spectroscopy (Inca X-max 50, Japan) for elemental analysis. To assess surface wettability, a contact angle goniometer (Biolin Theta, Germany) was utilized. The crystalline structures of the materials were characterized using both a small/wide angle scattering diffractometer (3.0 UHR Xeuss, France) and micro-Raman spectroscopy (InVia Renishaw, UK). Additionally, surface topography was examined using the tapping mode of an atomic force microscope (Bruker Dimension ICON).

Author contributions

J. S. and K. L. Y. conceived and designed the research. J. S., F. E. P. A., Z. X., X. W., and Q. W. conducted the experiments. J. S., M. L., and X. Y. analyzed the data. J. S. prepared the manuscript with direction, comments, and edits from W. H., M. K., Y. H., H.-J. B., and K. L. Y. K. L. Y. supervised the research.

Conflicts of interest

The authors declare no competing interests.

Data availability

The data supporting this article have been included as part of the ESI.†

Acknowledgements

Authors acknowledge the financial support from the Innovation Technology Fund (ITS/031/22MX, ITS/300/18), the European Union-Hong Kong Research Cooperation Co-funding Mechanism (E-HKUST601/17) from the Hong Kong Research Grants Council, the European Union's Horizon 2020 (BIORIMA), and the Project of Hetao Shenzhen-Hong Kong Science and Technology Innovation Cooperation Zone (HZQB-KCZYB-2020083), the National Science Foundation of China (no. 52276160). The authors acknowledge the support from Mr Cheuk Yin Tsang for material preparation, Miss Haoying Zhao for water condensation test, and Mr Liangchen Yang for theoretical condensation heat transfer analysis, and the Central Facilities of the Hong Kong University of Science and Technology including the Material Characterization and Preparation Facility (MCPF), the Environmental Central Facility (ENVF), the Nanosystem Fabrication Facility (CWB), and the Materials, Design and Manufacturing Facility (MDMF).

References

1 M. Jiang, Y. Wang, F. Liu, H. Du, Y. Li, H. Zhang, S. To, S. Wang, C. Pan, J. Yu, D. Quéré and Z. Wang, Inhibiting the Leidenfrost effect above 1000 °C for sustained thermal cooling, *Nature*, 2022, **601**(7894), 568–572.
2 X. Yan, F. Chen, S. Sett, S. Chavan, H. Li, L. Feng, L. Li, F. Zhao, C. Zhao, Z. Huang and N. Miljkovic, Hierarchical Condensation, *ACS Nano*, 2019, **13**(7), 8169–8184.
3 Y. Hou, P. Shah, V. Constantoudis, E. Gogolides, M. Kappl and H.-J. Butt, A super liquid-repellent hierarchical porous membrane for enhanced membrane distillation, *Nat. Commun.*, 2023, **14**(1), 6886.
4 J. B. Boreyko, Jumping droplets, *Droplet*, 2024, **3**(2), e105.
5 Y. Hou, Y. Shang, M. Yu, C. Feng, H. Yu and S. Yao, Tunable Water Harvesting Surfaces Consisting of Biphilic Nanoscale Topography, *ACS Nano*, 2018, **12**(11), 11022–11030.
6 Y. Gurumukhi, S. Chavan, S. Sett, K. Boyina, S. Ramesh, P. Sokalski, K. Fortelka, M. Lira, D. Park and J.-Y. Chen, Dynamic defrosting on superhydrophobic and biphilic surfaces, *Matter*, 2020, **3**(4), 1178–1195.
7 A. Hadžić, M. Može, M. Zupančič and I. Golobič, Superbiphilic Laser-Microengineered Surfaces with A Self-Assembled Monolayer Coating for Exceptional Boiling Performance, *Adv. Funct. Mater.*, 2024, **34**(10), 2310662.
8 C. Zhang, Z. Xu, N. Han, Y. Tian, T. Kallio, C. Yu and L. Jiang, Superaerophilic/superaerophobic cooperative electrode for efficient hydrogen evolution reaction *via* enhanced mass transfer, *Sci. Adv.*, 2023, **9**(3), eadd6978.
9 Y. Zhu, C. Y. Tso, T. C. Ho, M. K. Leung and S. Yao, Coalescence-induced jumping droplets on nanostructured biphilic surfaces with contact electrification effects, *ACS Appl. Mater. Interfaces*, 2021, **13**(9), 11470–11479.
10 K. Yang, R. Kas, W. A. Smith and T. Burdyny, Role of the carbon-based gas diffusion layer on flooding in a gas diffusion electrode cell for electrochemical CO_2 reduction, *ACS Energy Lett.*, 2020, **6**(1), 33–40.
11 G. Ren, M. Zhou, P. Hu, J.-F. Chen and H. Wang, Bubble-water/catalyst triphase interface microenvironment accelerates photocatalytic OER *via* optimizing semi-hydrophobic OH radical, *Nat. Commun.*, 2024, **15**(1), 2346.
12 H. Rabiee, L. Ge, J. Zhao, X. Zhang, M. Li, S. Hu, S. Smart, T. E. Rufford, Z. Zhu and H. Wang, Regulating the reaction zone of electrochemical CO_2 reduction on gas-diffusion electrodes by distinctive hydrophilic-hydrophobic catalyst layers, *Appl. Catal., B*, 2022, **310**, 121362.
13 R. Shi, J. Guo, X. Zhang, G. I. Waterhouse, Z. Han, Y. Zhao, L. Shang, C. Zhou, L. Jiang and T. Zhang, Efficient wettability-controlled electroreduction of CO2 to CO at Au/C interfaces, *Nat. Commun.*, 2020, **11**(1), 3028.
14 Y. Lin, T. Wang, L. Zhang, G. Zhang, L. Li, Q. Chang, Z. Pang, H. Gao, K. Huang and P. Zhang, Tunable CO_2 electroreduction to ethanol and ethylene with controllable interfacial wettability, *Nat. Commun.*, 2023, **14**(1), 3575.
15 S. H. Ko, D. Lee, H. W. Kang, K. H. Nam, J. Y. Yeo, S. J. Hong, C. P. Grigoropoulos and H. J. Sung, Nanoforest of hydrothermally grown hierarchical ZnO nanowires for a high efficiency dye-sensitized solar cell, *Nano Lett.*, 2011, **11**(2), 666–671.
16 L. E. Greene, M. Law, D. H. Tan, M. Montano, J. Goldberger, G. Somorjai and P. Yang, General route to vertical ZnO nanowire arrays using textured ZnO seeds, *Nano Lett.*, 2005, **5**(7), 1231–1236.
17 S. Anand and S. Y. Son, Sub-micrometer dropwise condensation under superheated and rarefied vapor condition, *Langmuir*, 2010, **26**(22), 17100–17110.
18 C. Dietz, K. Rykaczewski, A. Fedorov and Y. Joshi, Visualization of droplet departure on a superhydrophobic surface and implications to heat transfer enhancement during dropwise condensation, *Appl. Phys. Lett.*, 2010, **97**(3), 033104.
19 N. Miljkovic, R. Enright, Y. Nam, K. Lopez, N. Dou, J. Sack and E. N. Wang, Jumping-droplet-enhanced condensation on scalable superhydrophobic nanostructured surfaces, *Nano Lett.*, 2013, **13**(1), 179–187.
20 K. Rykaczewski, J. Scott and A. G. Fedorov, Electron beam heating effects during environmental scanning electron microscopy imaging of water condensation on superhydrophobic surfaces, *Appl. Phys. Lett.*, 2011, **98**(9), 093106.
21 R. Wen, Z. Lan, B. Peng, W. Xu, R. Yang and X. Ma, Wetting transition of condensed droplets on nanostructured superhydrophobic surfaces: coordination of surface properties and condensing conditions, *ACS Appl. Mater. Interfaces*, 2017, **9**(15), 13770–13777.
22 J. B. Boreyko and C. H. Chen, Self-propelled dropwise condensate on superhydrophobic surfaces, *Phys. Rev. Lett.*, 2009, **103**(18), 184501.
23 X. M. Chen, J. Wu, R. Y. Ma, M. Hua, N. Koratkar, S. H. Yao and Z. K. Wang, Nanograssed Micropyramidal Architectures for Continuous Dropwise Condensation, *Adv. Funct. Mater.*, 2011, **21**(24), 4617–4623.
24 H. Cha, C. Xu, J. Sotelo, J. M. Chun, Y. Yokoyama, R. Enright and N. Miljkovic, Coalescence-induced nanodroplet jumping, *Phys. Rev. Fluids*, 2016, **1**(6), 064102.

25 R. Wen, S. Xu, X. Ma, Y.-C. Lee and R. Yang, Three-Dimensional Superhydrophobic Nanowire Networks for Enhancing Condensation Heat Transfer, *Joule*, 2018, **2**(2), 269–279.
26 C. Ma, L. Chen, L. Wang, W. Tong, C. Chu, Z. Yuan, C. Lv and Q. Zheng, Condensation droplet sieve, *Nat. Commun.*, 2022, **13**(1), 5381.
27 L. Zhang, Z. Guo, J. Sarma, W. Zhao and X. Dai, Gradient quasi-liquid surface enabled self-propulsion of highly wetting liquids, *Adv. Funct. Mater.*, 2021, **31**(13), 2008614.
28 R. Mukherjee, A. S. Berrier, K. R. Murphy, J. R. Vieitez and J. B. Boreyko, How surface orientation affects jumping-droplet condensation, *Joule*, 2019, **3**(5), 1360–1376.
29 H. Cha, H. Vahabi, A. Wu, S. Chavan, M. K. Kim, S. Sett, S. A. Bosch, W. Wang, A. K. Kota and N. Miljkovic, Dropwise condensation on solid hydrophilic surfaces, *Sci. Adv.*, 2020, **6**(2), eaax0746.
30 J. Song, T. R. N. Dy, M. Li, X. Yan, H. Zhao, Z. Zhang, S. Taghipour, N. Zhan and K. L. Yeung, Sustainable Water Management with Photocatalytic Janus Mesh: Efficient Fog Harvesting, Water Purification, and Microbial Disinfection, *ACS Appl. Mater. Interfaces*, 2024, **16**(44), 61331–61343.
31 Y. L. A. Leung and K. Yeung, Microfabricated ZSM-5 zeolite micromembranes, *Chem. Eng. Sci.*, 2004, **59**(22–23), 4809–4817.
32 Y. S. S. Wan, J. L. H. Chau, A. Gavriilidis and K. L. Yeung, TS-1 zeolite microengineered reactors for 1-pentene epoxidation, *Chem. Commun.*, 2002, (8), 878–879.
33 W. Lau, K. L. Yeung and R. Martin-Aranda, Knoevenagel condensation reaction between benzaldehyde and ethyl acetoacetate in microreactor and membrane microreactor, *Microporous Mesoporous Mater.*, 2008, **115**(1–2), 156–163.
34 K. L. Yeung and W. Han, Zeolites and mesoporous materials in fuel cell applications, *Catal. Today*, 2014, **236**, 182–205.
35 R. Deng, W. Han and K. L. Yeung, Confined PFSA/MOF composite membranes in fuel cells for promoted water management and performance, *Catal. Today*, 2019, **331**, 12–17.
36 L. T. Y. Au, W. Y. Mui, P. S. Lau, C. T. Ariso and K. L. Yeung, Engineering the shape of zeolite crystal grain in MFI membranes and their effects on the gas permeation properties, *Microporous Mesoporous Mater.*, 2001, **47**(2–3), 203–216.
37 W. C. Wong, L. T. Y. Au, P. P. Lau, C. T. Ariso and K. L. Yeung, Effects of synthesis parameters on the zeolite membrane morphology, *J. Membr. Sci.*, 2001, **193**(2), 141–161.
38 T. A. D. Peña, R. Ma, Z. Xing, Q. Wei, J. I. Khan, R. M. Young, Y. Hai, S. A. Garcia, X. Zou and Z. Jin, Interface property–functionality interplay suppresses bimolecular recombination facilitating above 18% efficiency organic solar cells embracing simplistic fabrication, *Energy Environ. Sci.*, 2023, **16**(8), 3416–3429.
39 N. Yao and K. L. Yeung, Investigation of the performance of TiO2 photocatalytic coatings, *Chem. Eng. J.*, 2011, **167**(1), 13–21.
40 X. Wang, X. Zhang, Y. Wang, H. Liu, J. Qiu, J. Wang, W. Han and K. L. Yeung, Investigating the role of zeolite nanocrystal seeds in the synthesis of mesoporous catalysts with zeolite wall structure, *Chem. Mater.*, 2011, **23**(20), 4469–4479.
41 X. Wang, X. Zhang, Y. Wang, H. Liu, J. Qiu, J. Wang, W. Han and K. L. Yeung, Performance of TS-1-coated structured packing materials for styrene oxidation reaction, *ACS Catal.*, 2011, **1**(5), 437–445.
42 M. Li, C.-H. Mo, X. Luo, K.-Y. He, J.-F. Yan, Q. Wu, P.-F. Yu, W. Han, N.-X. Feng and K. L. Yeung, Exploring key reaction sites and deep degradation mechanism of perfluorooctane sulfonate *via* peroxymonosulfate activation under electrocoagulation process, *Water Res.*, 2021, **207**, 117849.
43 M. Li, Z. Li, X. Yu, Y. Wu, C. Mo, M. Luo, L. Li, S. Zhou, Q. Liu and N. Wang, FeN_4-doped carbon nanotubes derived from metal organic frameworks for effective degradation of organic dyes by peroxymonosulfate: Impacts of FeN_4 spin states, *Chem. Eng. J.*, 2022, **431**, 133339.